ACS OMEGA

http://pubs.acs.org/journal/acsodf

Article

Nanoencapsulation as a Promising Platform for the Delivery of the Morin-Cu(II) Complex: Antibacterial and Anticancer Potential

Pooja Ghosh, Sudipta Bag, Sultana Parveen, Elavarasan Subramani, Koel Chaudhury, and Swagata Dasgupta*

Cite This: *ACS Omega* 2022, 7, 7931−7944

Read Online

ACCESS | Metrics & More | Article Recommendations | Supporting Information

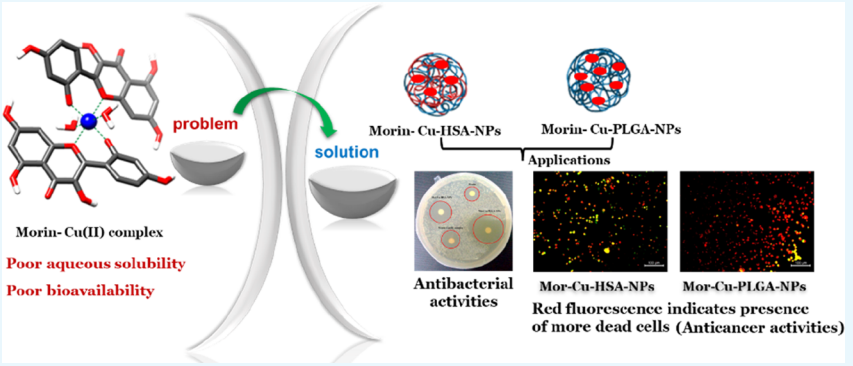

ABSTRACT: Nanoencapsulation has emerged as a promising approach for the effective delivery of poorly aqueous soluble compounds. The current study focuses on the preparation of human serum albumin (HSA)-based nanoparticles (NPs) and poly lactic-*co*-glycolic acid (PLGA)-based nanoparticles for effective delivery of the morin-Cu(II) complex. The NPs were analyzed based on different parameters such as particle size, surface charge, morphology, encapsulation efficiency, and *in vitro* release properties. The average particle sizes were found to be 214 ± 6 nm for Mor-Cu-HSA-NPs and 185 ± 7.5 nm for Mor-Cu-PLGA-NPs. The release of the morin-Cu(II) complex from both the NPs (Mor-Cu-HSA-NPs and Mor-Cu-PLGA-NPs) followed a biphasic behavior, which comprises an early burst release followed by a sustained and controlled release. The resulting NPs also exhibit free radical scavenging activity confirmed by a standard antioxidant assay. The antibacterial activities of the NPs were investigated using a disk diffusion technique, and it was observed that both the NPs showed better antibacterial activity than morin and the morin-Cu(II) complex. The anticancer activities of the prepared NPs were examined on MDA-MB-468 breast cancer cell lines using a cytotoxicity assay, and the mode of cell death was visualized using fluorescence microscopy. Our results revealed that NPs kill the cancer cells with greater efficiency than free morin and the morin-Cu(II) complex. Thus, both HSA-based NPs and PLGA-based NPs can act as promising delivery systems for the morin-Cu(II) complex and can be utilized for further biomedical applications.

INTRODUCTION

Flavonoids, a group of polyphenolic compounds, are abundantly found in several fruits, vegetables, seeds, and herbs and possess various biological activities including antioxidant, anti-inflammatory, and anticarcinogenic activities.[1−3] Many flavonoids act as natural chelators. The specific chemical scaffold comprising mainly carbonyl and hydroxyl groups present in flavonoids makes it suitable for favorable chelation with metal ions and forming flavonoid−metal complexes. Flavonoid−metal complexes are utilized as colorimetric reagents for the determination of metal ions.[4,5] Several studies have corroborated that the antioxidant behavior of flavonoids is due to their chelating properties. Flavonoid−metal chelates are found to be more powerful free radical scavengers than the free flavonoids and play a pivotal role in preventing radical generation and thus providing protection from oxidative stress. They also exhibit higher cytotoxic activity than the parent flavonoids. Furthermore, complexes of flavonoids have an enormous impact in controlling metal bioavailability and preventing metal toxicity. Among the several metal ions, copper plays a key role in the formation of a reactive hydroxyl radical (HO) through the Fenton and Haber−Weiss reactions. Due to the redox nature of copper, it is involved in various biological processes including regulation of hemoglobin level, embryonic development, mitochondrial

Received: December 9, 2021
Accepted: February 9, 2022
Published: February 22, 2022

respiration, and physiological processes such as iron metabolism, cellular respiration, free radical detoxification, etc.[6−8] Copper is also an important cofactor in several metabolic pathways. Plant pathogenic fungi and bacteria on agricultural crops can be controlled by using copper-containing compounds like copper sulfate, Bordeaux mixtures, etc. The toxicity of copper can be reduced by coordination of copper with natural chelating agents.

Morin hydrate (3,5,7,2′,4′-pentahydroxyflavone) is a flavonol (Figure 1), which belongs to the flavonoid group. It

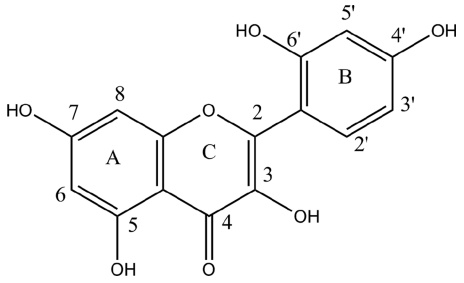

Figure 1. Molecular structure of morin.

is mainly present in guava leaves, onion, red wine, herbs, fruit, and other *Moraceae*.[9−11] Morin is also used as a food preservative. It is extensively used as a probe for metal ion detection and detection of other biomacromolecules like nucleic acids, proteins,[12] etc. It has been reported that coordination of flavonoids like quercetin and morin with metals such as Cu(II) enhances the pharmaceutical activity of drugs and also diminishes their toxic effects.[13] Coordination of morin with Cu(II), Pt(II), La(III), and Gd(III) showed stronger antioxidant activity than morin alone. Because of the antioxidant nature of morin complexes, it also showed stronger inhibition property against three strains of bacteria, e.g., *Escherichia coli*, *Klebsiella pneumonia*, and *Staphylococcus aureus*.[14]

Due to the interesting properties of both morin and copper, we have synthesized the morin-Cu(II) complex in our present work. However, one of the major limitations of the morin-Cu(II) complex is its low aqueous solubility, which restricts its applications in clinical and biopharmaceutical fields. To overcome this shortcoming, we have prepared nanoparticles of the morin-Cu(II) complex to check the stabilization and solubilization, which in turn is expected to improve its therapeutic efficacy. The past few years have seen a rise in the usage of nanoparticles as drug delivery systems due to their widespread applications in pharmaceutical and biomedical fields. Researchers have found interest in designing nanoparticles because of their unique properties including chemical, mechanical, electrical, optical, magnetic, electro-optical, and magneto-optical properties. All these properties make the nanoparticles useful in the field of biomedical applications particularly as delivery systems and in imaging. Ongoing research is being carried out to attempt new formulations that are able to deliver drugs to specific target areas of the body. Herein, we choose a nanoencapsulation technique for improving the solubility and delivering this poorly aqueous soluble compound, the principle of which may be adopted for other such similar compounds/drugs as well. A proper selection of matrix is vital in this regard to obtain a better nanoparticulate delivery system. Several matrices such as proteins, polysaccharides, polymers, and liposomes have been already exploited by researchers because of their numerous advantages, which make them suitable drug delivery vehicles.[15−17] In our present study, we have chosen two different carriers, human serum albumin (HSA) and poly lactic-*co*-glycolic acid (PLGA), to synthesize nanoparticles. HSA was chosen as the matrix for nanoparticle formation owing to its easy availability, biocompatible nature, biodegradability, lack of toxicity, reproducibility, and non-antigenicity. PLGA has also been used by several researchers as a carrier in the preparation of nanoparticles. As PLGA is biodegradable, biocompatible, and non-toxic, we have also chosen PLGA as one of the components of our matrix. Hydrolysis of PLGA leads to the formation of natural biodegradable metabolites (lactic acid and glycolic acid), which can be easily metabolized in our body *via* Krebs cycle and eliminated from our body as carbon dioxide and water. Both HSA and PLGA have been accepted by the US Food and Drug Administration and European Medicine Agency for human use.

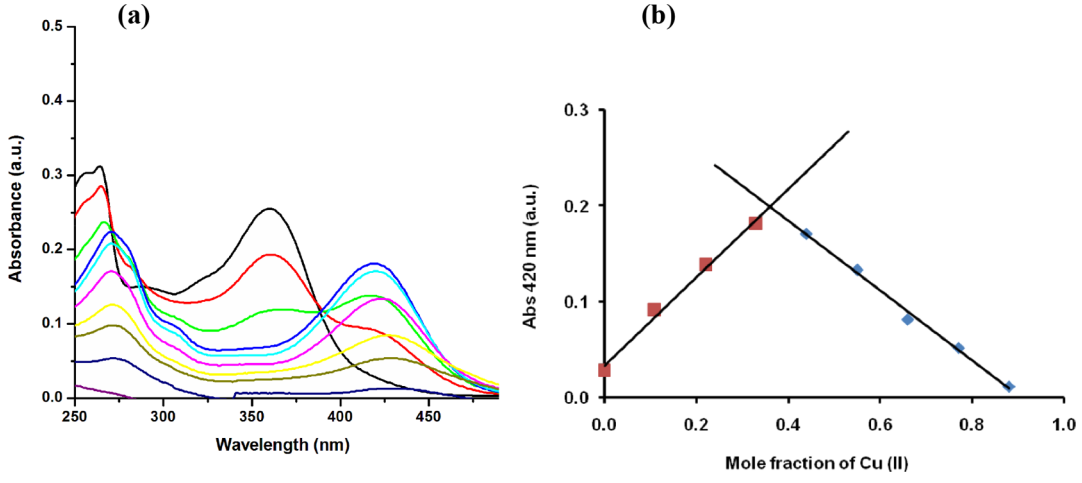

Figure 2. (a) UV−vis absorption spectra of morin in the presence of Cu(II) ion in HPLC-grade ethanol. Job's continual variation methods applied for the complexation between morin and Cu(II) ion. Metal-to-ligand molar ratios varying from 1:7 to 7:1 in ethanol. (b) Corresponding Job's plot indicating 2:1 morin to Cu(II) complexation.

https://doi.org/10.1021/acsomega.1c06956
ACS Omega 2022, 7, 7931−7944

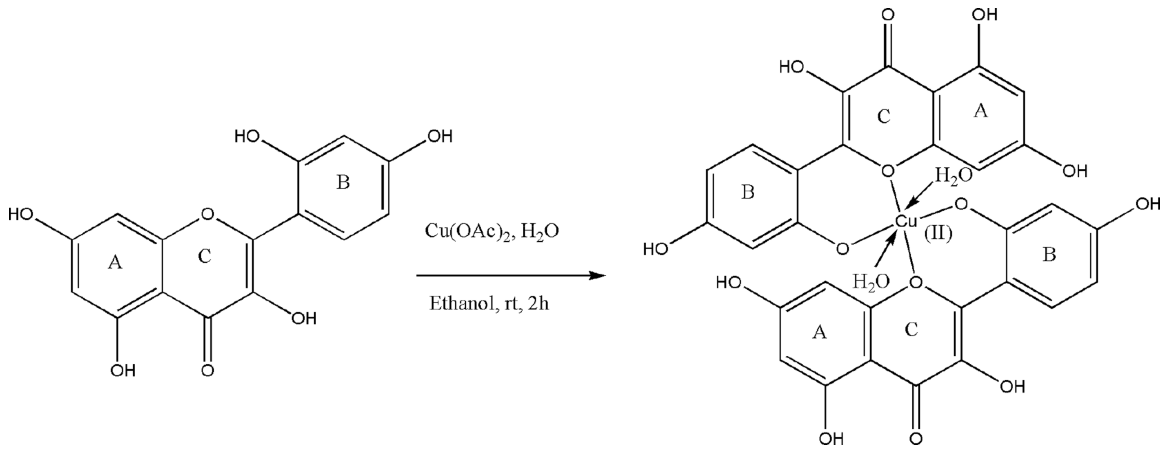

Figure 3. Schematic representation of the complexation of morin with $Cu(OAc)_2 \cdot H_2O$.

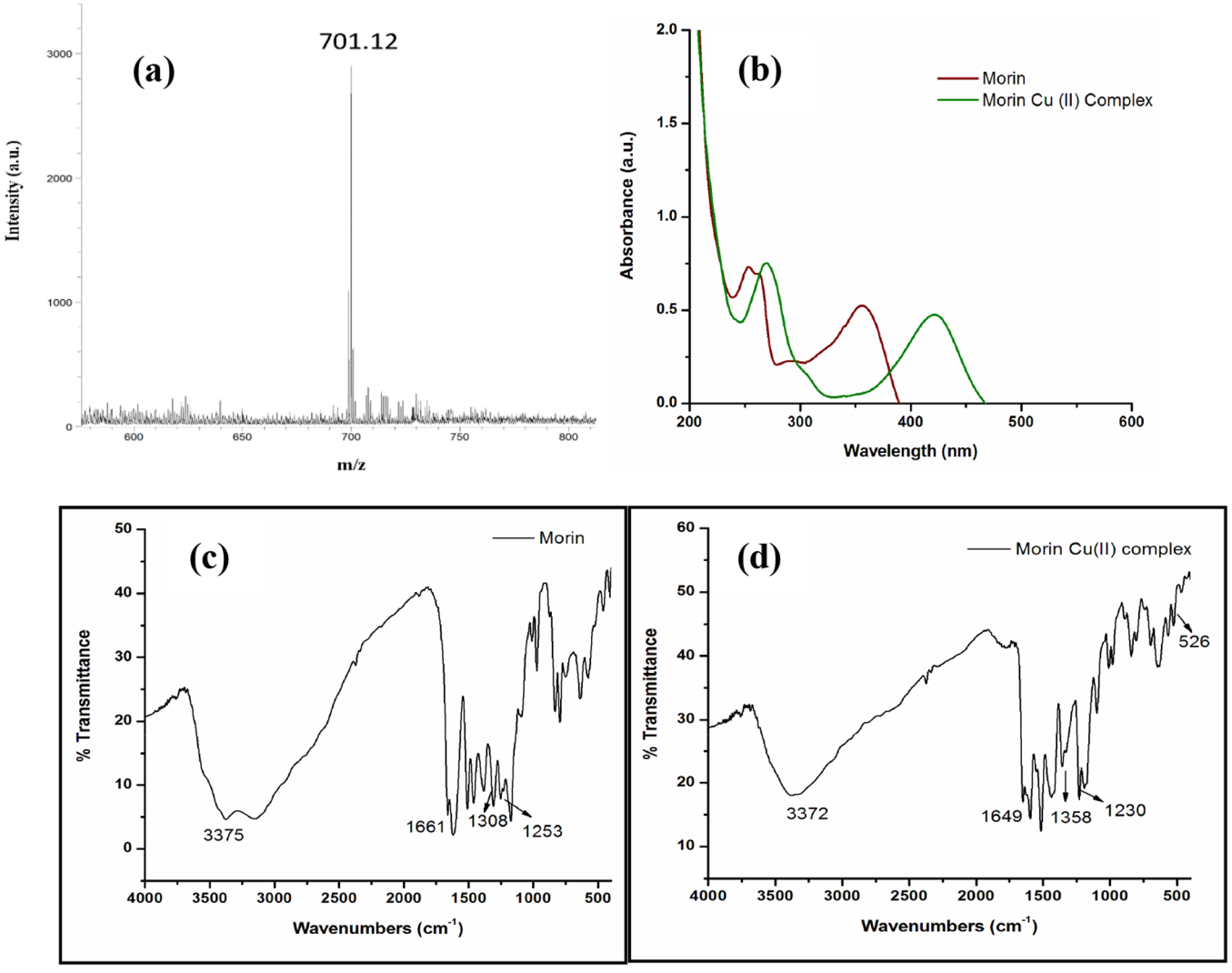

Figure 4. (a) MALDI-TOF spectra of morin-Cu(II) complex. (b) UV−vis absorption spectra of morin and morin-Cu(II) complex. FTIR spectra of (c) morin and (d) morin-Cu(II) complex

In this context, this work is aimed at the preparation of nanoparticles of the morin-Cu(II) complex using two different matrices. The complex was prepared and characterized by standard spectroscopic techniques. The nanoparticles of the morin-Cu(II) complex were then prepared using a desolvation technique (HSA matrix) and an S/O/W emulsification technique (PLGA matrix). Characterization of the nanoparticles involved surface morphology and size distribution measurements. Encapsulation efficiency and release properties *in vitro* were also tested in this study. The antioxidant activity

https://doi.org/10.1021/acsomega.1c06956
ACS Omega 2022, 7, 7931−7944

of the nanoparticles was determined using a 2,2-diphenyl-1-picrylhydrazyl (DPPH) assay. The toxicity of the nanoparticles was checked using a hemolytic assay. Further, the antibacterial activities of the NPs were determined using a disk diffusion technique and the efficacy of nanoparticles toward breast cancer cell lines was evaluated. The present findings add to the knowledge of drug delivery applications and could be further explored to aid in the design of novel effective drug delivery vehicles.

RESULTS AND DISCUSSION

Nanocarriers have been designed to improve the solubility and bioavailability of many drugs that suffer from poor aqueous solubility. In our present study, we have used two different matrices, HSA and PLGA, to prepare the NPs in order to increase the solubility of the morin-Cu(II) complex.

Determination of Stoichiometric Ratio: Job's Plot. Prior to the preparation of the morin-Cu(II) complex, the stoichiometric ratio between Cu(II) and morin was determined according to Job's continual variation method.[18] The absorbance at 420 nm (λ_{max}) was plotted against the mole fraction of the Cu(II) ion (Figure 2). The graph indicated that the molar ratio involved in the formation of the morin-Cu(II) complex is 2:1.

Synthesis and Characterization of the Morin-Cu(II) Complex. The morin-Cu(II) complex was synthesized using a previous method resulting in the formation of a dark-chocolate-colored compound.[43] A schematic representation of the complexation of morin with $Cu(OAc)_2{\cdot}H_2O$ is shown in Figure 3. Elemental analysis shows % C = 51.25 and % H = 3.29, whereas the theoretical values are % C = 51.33 and % H = 3.16. The calculated atomic mass for $[CuC_{30}H_{22}O_{16}]$ is 701.0304, and the mass obtained from MALDI-TOF spectra (Figure 4a) is found to be m/z 701.12. This result is in agreement with the proposed structure of the copper complex. UV−vis spectra show two distinct bands of morin at 351 nm (band I) and 264 nm (band II) due to the cinnamoyl moiety and the benzoyl moieties, respectively. The formation of the morin-Cu(II) complex results in a bathochromic shift of band I (Figure 4b). The increase in conjugation in the complex results in this distinct shift, which further indicates that the 2′-OH group of ring B is involved in the formation of the morin-Cu(II) complex.[43] The complex formation has also been characterized using FTIR spectroscopy (Figure 4c,d), and the wavenumbers of the bands of morin and the morin-Cu(II) complex are shown in Table 1.

The formation of the morin-Cu(II) complex results in an increase in the stretching frequency of the C−O−H mode from 1308 to 1360 cm^{-1}, which indicates that the ortho-phenolic moiety on the B ring of morin is involved in chelation with the Cu(II) ion.[19] In the morin-Cu(II) complex, the Cu−O stretching vibration appears at 526 cm^{-1}, whereas no such band appears in the case of morin alone, which confirms the formation of the metal complex. Further, a noticeable decrease of 23 cm^{-1} in the C−O−C stretching frequency of the morin-Cu(II) complex was observed, which implies the participation of oxygen of the C ring during complex formation.[20] A broad band in the range 3450−3064 cm^{-1} appears due to the O−H stretching frequency, which indicates the presence of water molecules in the complex. The energy optimized structure of the morin-Cu(II) complex is given in Figure 5.

Table 1. Assignment of the Main IR Bands of Morin and Morin-Cu(II) Complex

bands (cm^{-1})	morin	morin-Cu(II) complex
$\nu_{C=O}$	1661 (s)	1649 (s)
ν_{C-O-C}	1253 (s)	1230 (s)
ν_{M-O}		526 (s)
$\nu_{C2'-OH}$	1308 (s)	1358 (s)
ν_{O-H}	3375 (b)	3372 (b)

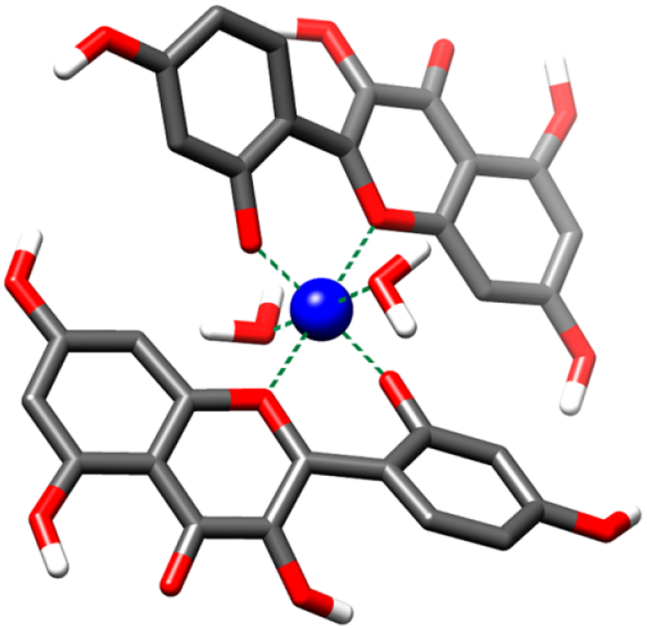

Figure 5. Energy-optimized structure of the morin-Cu(II) complex.

PREPARATION AND CHARACTERIZATION OF NPS

HSA-based NPs were prepared using a desolvation technique, whereas PLGA-based NPs were prepared using an S/O/W emulsification technique. The desolvation technique involves ethanol addition, which causes phase separation. Due to the desolvating nature of ethanol, it decreases the solubility of HSA in water and promotes the aggregation of the protein molecules in the aqueous phase. Glutaraldehyde, a cross-linking agent, was also added to the solution, which imparts stability to the NPs. The S/O/W emulsification technique involves addition of an oil phase into a water phase where the morin-Cu(II) complex and PLGA in acetone were used as the oil phase and PVA solution used as the water phase.

SPECTROSCOPIC CHARACTERIZATION

UV−vis Spectroscopy. To observe the change in spectral properties of the morin-Cu(II) complex after encapsulation into the two different matrices (HSA and PLGA), a UV−vis study was performed. Figure 6 shows the UV−vis spectra of Mor-Cu-HSA-NPs and Mor-Cu-PLGA-NPs. The existence of both peaks of the morin-Cu(II) complex in the HSA and PLGA NPs indicates that the chemical structure of the morin-Cu(II) complex does not alter after encapsulation into the matrices.

FTIR Study. The interaction between the morin-Cu(II) complex and the matrix (HSA and PLGA) was investigated by an FTIR analysis. For HSA, the amide I and amide II bands

https://doi.org/10.1021/acsomega.1c06956
ACS Omega 2022, 7, 7931−7944

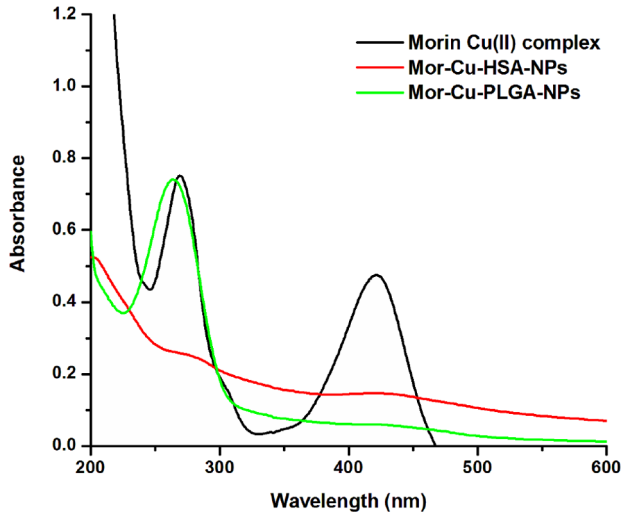

Figure 6. UV−vis absorption spectra of Mor-Cu-HSA-NPs and Mor-Cu-PLGA-NPs.

appear at 1654 and 1550 cm^{-1}, respectively. The amide I band is due to the C═O stretching frequency, whereas the amide II band is due to the C−N stretching coupled with N−H bending. For PLGA, the band at 1757 cm^{-1} is due to the C═O stretching frequency and the bands at 1044 and 1248 cm^{-1} involve the C−O stretching frequency. FTIR results of morin and the morin-Cu(II) complex are in Table 1. The FTIR spectra of NPs are presented in Figure 7 where the spectra of both Mor-Cu-HSA-NPs and Mor-Cu-PLGA-NPs contain the characteristic bands of the morin-Cu(II) complex with a slight shift. The $\nu_{C2'-OH}$ of the morin-Cu(II) complex shifts from 1358 to 1362 cm^{-1} (for Mor-Cu-HSA-NPs) and 1365 cm^{-1} (for Mor-Cu-PLGA-NPs), whereas ν_{C-O-C} of the morin-Cu(II) complex shifts from 1230 to 1232 cm^{-1} (for Mor-Cu-HSA-NPs) and 1236 cm^{-1} (for Mor-Cu-PLGA-NPs). Further, ν_{Cu-O} of the morin-Cu(II) complex shifts from 526 to 524 cm^{-1} (for Mor-Cu-HSA-NPs) and 530 cm^{-1} (for Mor-Cu-PLGA-NPs). Our results are also an indication of the superposition of the matrix (HSA and PLGA) and the morin-Cu(II) complex, which implies that the morin-Cu(II)

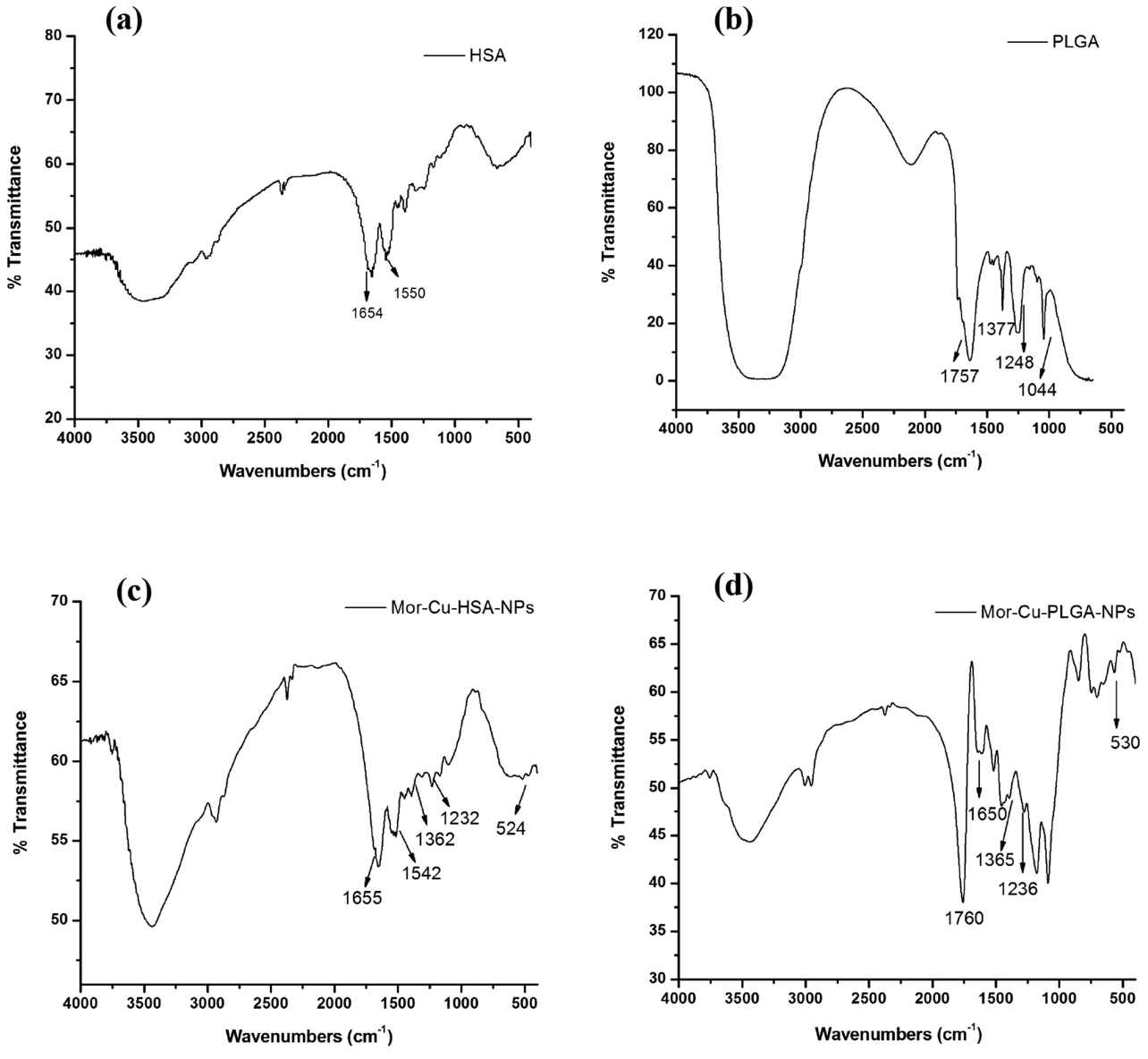

Figure 7. FTIR Spectra of (a) HSA, (b) PLGA, (c) Mor-Cu-HSA-NPs, and (d) Mor-Cu-PLGA-NPs.

https://doi.org/10.1021/acsomega.1c06956
ACS Omega 2022, 7, 7931−7944

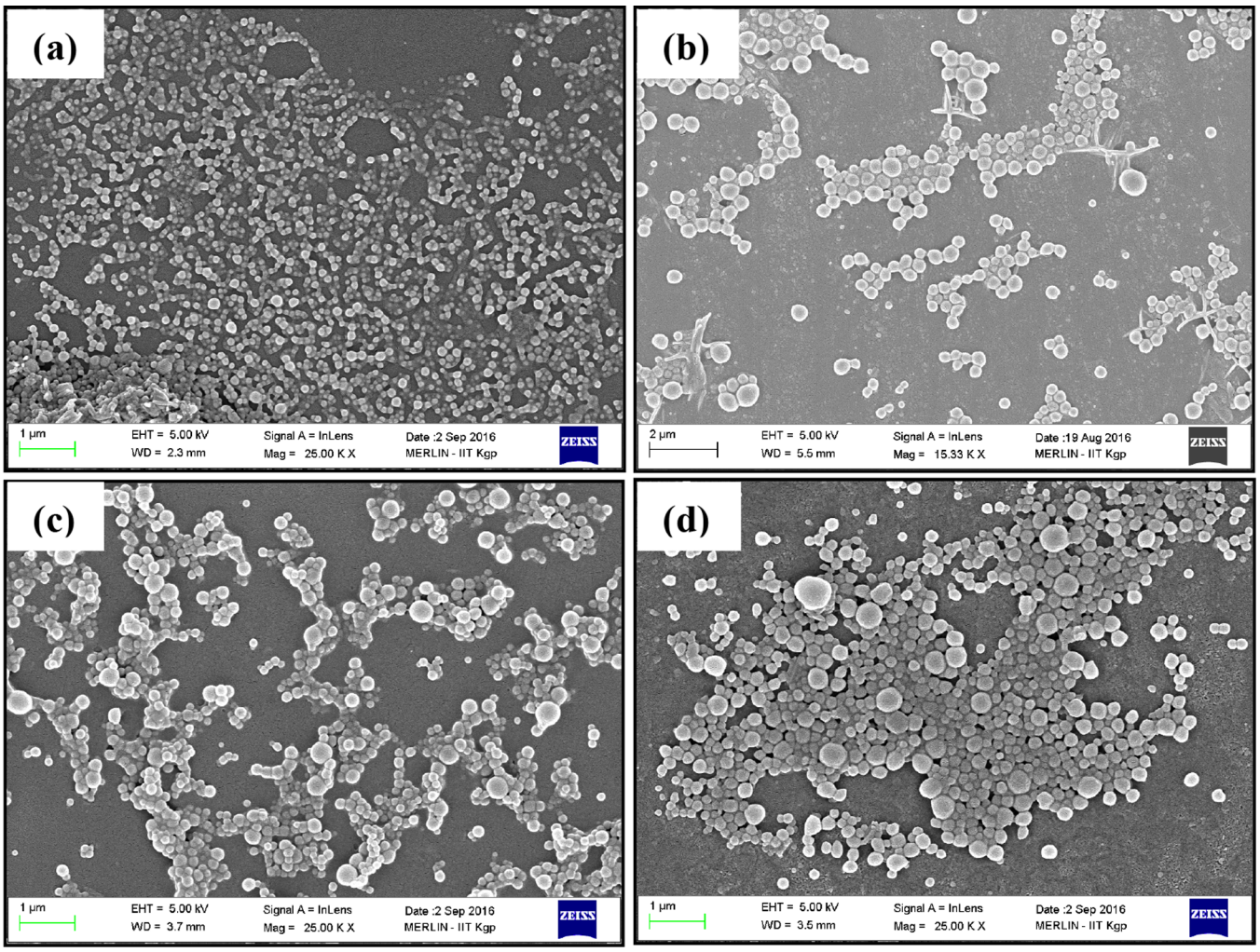

Figure 8. FESEM images of (a) HSA NPs, (b) Mor-Cu-HSA-NPs, (c) PLGA NPs, and (d) Mor-Cu-PLGA-NPs.

complex is entrapped within the matrix (HSA and PLGA) without affecting its chemical structure. This observation is in accordance with previous literature reports.[21,22] Similar types of results have already been shown from this laboratory,[23−25] and the present findings are consistent with the earlier studies.

Morphological Characterization and Determination of Sizes and Surface Charge. Field emission scanning electron microscopy (FESEM) was used for morphological characterization of the nanoparticles. FESEM images display almost a uniform and spherical type morphology of the prepared NPs with a smooth surface (Figure 8). The surface topography of the prepared NPs was also investigated by AFM analyses. As shown in Figure 9, we have observed a smooth spherical appearance of NPs, which confirms the observation obtained from the FESEM results.

Particle size in addition to size distributions play a critical role in physicochemical properties of nanoparticle systems such as drug loading and release properties, stability, etc.[26] Cellular uptake properties as well as bioavailability of drugs are also influenced by the sizes of the particles. Thus, it is important to control the size of the particles. In a desolvation technique, several parameters such as pH and percentage of ethanol addition influence the sizes of the particles. Acidic pH results in the formation of larger particles, while an increase in pH value decreases the particle sizes. In our present work, we have prepared the NPs using a pH value of 8.5. The increase in

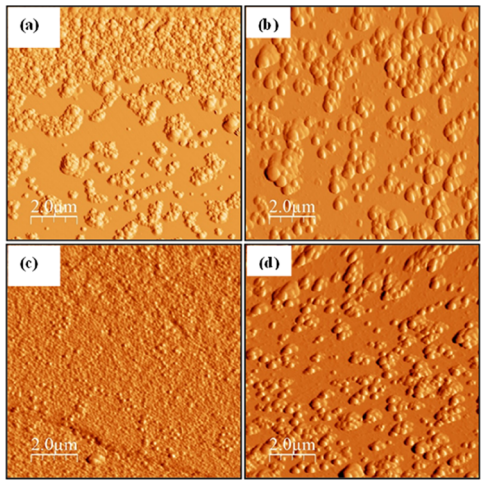

Figure 9. AFM images of (a) HSA NPs, (b) Mor-Cu-HSA-NPs, (c) PLGA NPs, and (d) Mor-Cu-PLGA-NPs.

the percentage of ethanol results in a gradual decrease in the particle size. In the present study, we have obtained the NPs using 70% ethanol. In the solid in oil in water (S/O/W) emulsification technique, the PLGA content, surfactant content, aqueous-to-organic phase volume ratio, etc. affect the particle sizes. Previous reports indicate that the particles

https://doi.org/10.1021/acsomega.1c06956
ACS Omega 2022, 7, 7931−7944

with average sizes around 300 nm or smaller than 300 nm can be easily delivered to the target site through the human body. The size distribution profile (DLS profile) is shown in Figure S1 of the Supporting Information. The results (Table 2) showed that the average sizes of the particles are ∼214 ± 6 nm for Mor-Cu-HSA-NPs and ∼185 ± 7.5 nm for Mor-Cu-PLGA-NPs.

Table 2. Average Sizes, Polydispersity Index, and Zeta Potential Values of Different Samples

sample	average sizes (nm)	polydispersity index	zeta potential (mV)
Mor-Cu-HSA-NPs	214 ± 6	0.521	−23.4 ± 0.9
Mor-Cu-PLGA-NPs	185 ± 7.5	0.454	−27.2 ± 1.1

Further, the surface charge of the NPs was determined by zeta potential measurements. The zeta potential is a crucial factor for estimating the stability of the colloidal dispersion.[27] The magnitude of zeta potential indicates the repulsive force present in the colloidal nanoparticle dispersion. It has been observed that particles having a zeta potential value above ±30 mV are stable because of the electric repulsion between the particles.[28] From zeta potential measurements (Table 2), we have observed that the surface charge of both the NPs is negative. The average zeta potential value of Mor-Cu-HSA-NPs is found to be −23.4 ± 0.9 mV and that of Mor-Cu-PLGA-NPs is −27.2 ± 1.1 mV, which indicates an overall higher stability of the NPs. Zeta potential distribution of Mor-Cu-HSA-NPs and Mor-Cu-PLGA-NPs are shown in Figure S2.

Encapsulation Efficiency. To calculate the encapsulation efficiency of the morin-Cu(II) complex in HSA-based NPs and PLGA-based NPs, both the NPs were centrifuged and the absorbance of the supernatant was recorded using UV−vis spectroscopy. Our study showed ∼87% encapsulation efficiency for HSA-based NPs and 82% encapsulation efficiency for PLGA-based NPs.

***In Vitro* Release Study.** There are several factors that influence the drug release rate. These factors include solubility of drug, diffusion through the matrix, erosion of the matrix, desorption from the adsorbed drug, etc. In our present study, the release of the morin-Cu(II) complex from HSA-based NPs and PLGA-based NPs was carried out using a dialysis technique over a period of 96 h. As shown in Figure 10, the release of the morin-Cu(II) complex from both HSA-based and PLGA-based NPs followed a biphasic release pattern. The biphasic release pattern comprises a burst release in the initial period followed by a slow and sustained release. The burst release in the initial period may be because of the small amount of the morin-Cu(II) complex adsorbed on the surface of the matrix, which results in the faster release in the initial stage. However, the morin-Cu(II) complex entrapped within the NPs causes slow and sustained release. The drug release profiles in PBS (pH 7.4) shown in Figure 10a indicate that the total release at the end of 96 h is found to be ∼71% for Mor-Cu-HSA-NPs and ∼75% for Mor-Cu-PLGA-NPs. In addition, the release of the morin-Cu(II) complex has been monitored in an acidic pH medium (pH 6.5) under extracellular tumoral conditions. The total release at the end of 96 h is found to be ∼82% for Mor-Cu-HSA-NPs and ∼86% for Mor-Cu-PLGA-NPs (Figure 10b).

Antioxidant Activity. The DPPH assay is a widely used technique for determining the antioxidant potential of any

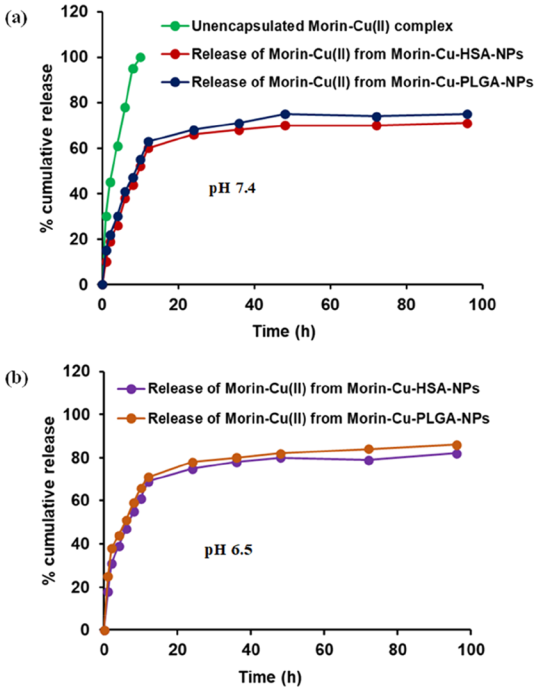

Figure 10. *In vitro* release profile of the morin-Cu(II) complex from Mor-Cu-HSA-NPs and Mor-Cu-PLGA-NPs at (a) pH 7.4 and (b) pH 6.5.

compound. DPPH is a nitrogen-centered stable free radical showing a maximum absorbance at 517 nm. Morin is well-known for its antioxidant property, and the antioxidant potential is due to its hydrogen-donating ability. Generally, the molecular structure and different spatial arrangement of hydroxyl groups regulate the antioxidant potential of polyphenols. An important feature of morin that is responsible for its antioxidant capacity is the presence of 3-OH groups attached to the 2,3-double bond and adjacent to the 4-carbonyl group in the C ring (Figure 1). In addition, the presence of both 3-OH and 5-OH groups along with the 4-carbonyl group in morin results in the formation of a catechol-like moiety in the C ring through intramolecular rearrangement. This is also an important criterion for its higher antioxidant capacity. When the prepared NPs (Mor-Cu-HSA-NPs and Mor-Cu-PLGA-NPs) were treated with DPPH solution, the purple color of DPPH turns pale yellow, which is an indication of the antioxidant potential of the NPs. Our findings reveal that the percentage of inhibition of DPPH by Mor-Cu-HSA-NPs is ∼79% and that of Mor-Cu-PLGA-NPs is ∼83%. The associated histogram of the percentage of inhibition is presented in Figure 11.

Hemolytic Assay. A hemolytic assay was performed to confirm whether the prepared NPs are toxic toward RBCs. Hemolysis is the process of rupturing of red blood cells, which allows hemoglobin to be released into the blood plasma. Hemolysis is responsible for several pathological conditions such as anemia, jaundice, renal toxicity, hypertension, etc.[29] For the use of NPs particularly in clinical applications, it is important to consider their hemolytic properties. According to ISO/TR 7405-1984(f), the samples are treated as non-hemolytic if the hemolytic percentage is found to be less than 5%. Samples having hemolytic values in between 5 and 10% are considered as slightly hemolytic, while the values higher than 10% are highly hemolytic. In our case, we have

https://doi.org/10.1021/acsomega.1c06956
ACS Omega 2022, 7, 7931−7944

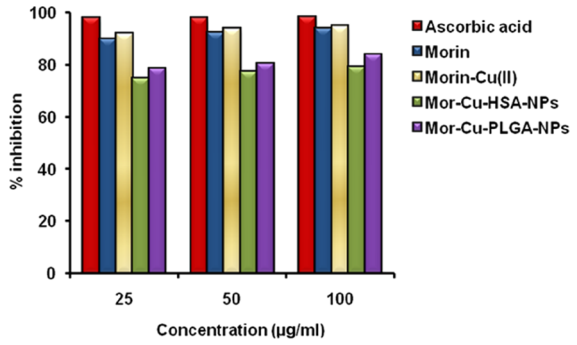

Figure 11. Histogram of percentage of inhibition of Mor-Cu-HSA-NPs and Mor-Cu-PLGA-NPs.

observed a hemolytic value of ∼1.4% for Mor-Cu-HSA-NPs and ∼0.9% for Mor-Cu-PLGA-NPs, indicating the non-hemolytic properties of both the NPs (Table 3). The non-toxic nature of both the NPs toward RBCs makes the NPs applicable for further biomedical investigations.

Table 3. Hemolytic Rate of Different Samples

sample	hemolytic percentage
morin-Cu(II) complex	2.5
Mor-Cu-HSA-NPs	1.4
Mor-Cu-PLGA-NPs	0.9

Antibacterial Activity. The antibacterial activities of both the NPs (Mor-Cu-HSA-NPs and Mor-Cu-PLGA-NPs) were evaluated by a disk diffusion technique using *Staphylococcus aureus* as the test bacteria. In our current study, *Staphylococcus aureus* (*S. aureus*) was chosen as the model bacteria for analyzing the potential of prepared nanoparticles on microbial organisms as it is the most significant bacteria and responsible for several infections, skin diseases, nosocomial infections, and food poisoning and are internalized in phagocytic cells. Figure 12 shows the disk diffusion test results of morin, morin-Cu(II) complex, Mor-Cu-HSA-NPs, and Mor-Cu-PLGA-NPs. The inhibitory zone was found to be 29 mm for Mor-Cu-HSA-NPs and 42 mm for Mor-Cu-PLGA-NPs (Table 4). The inhibition zones of nanoparticles are found to be increased compared to morin and morin-Cu(II) complex. The results indicated that the NPs were more effective than morin and morin-Cu(II) complex against *S. aureus*. The minimal inhibitory concentration (MIC) of morin-Cu(II) complex, Mor-Cu-HSA-NPs, and Mor-Cu-PLGA-NPs were observed at 15, 12, and 5 μg/mL, respectively. We have also analyzed the effect of HSA, PLGA, HSA NPs, and PLGA NPs against the test bacteria, and the results revealed that they did not show any antibacterial effect. The better antibacterial activity of the NPs compared to morin and morin-Cu(II) complex is most likely due to the better ability of the nanoparticles to transport and internalize higher concentrations of the complex in micro-organisms and cells.

Cytotoxicity Assay. Flavonoids are well-known for their anticancer activities. They have shown cytotoxic activity toward different cancer cell lines. A number of flavonoids such as quercetin,[30] fisetin,[31] apigenin,[32] genistein,[33] and luteolin[34] have been found to possess anticancer activity. The anticancer activity of flavonoids depends on several factors like structures, concentrations, and types of cell lines used. According to "Lipinski's rule of five",[35] if a compound contains

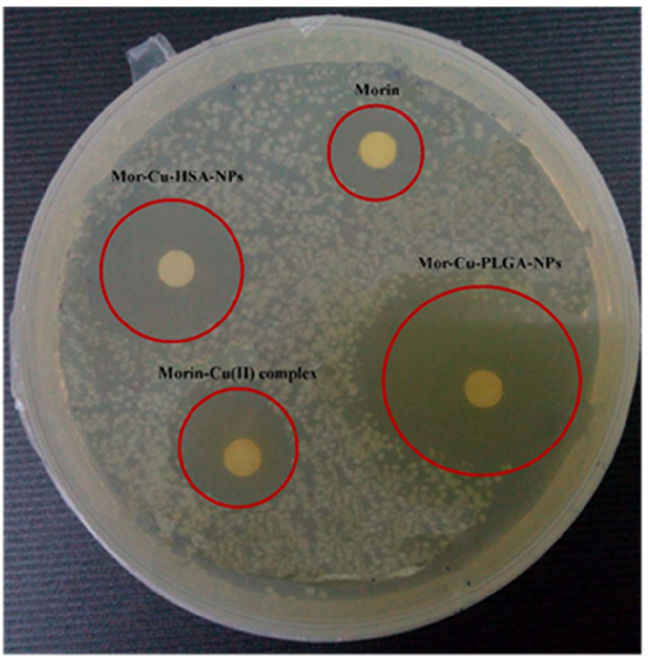

Figure 12. Inhibition zones of *S. aureus* in plates containing morin, morin-Cu(II) complex, Mor-Cu-HSA-NPs, and Mor-Cu-PLGA-NPs

Table 4. Quantitative Values of Inhibitory Zone against *S. aureus* and MIC of the Samples

sample	diameter of inhibitory zone (mm)	MIC (μg/mL)
morin-Cu(II) complex	20 ± 0.8	15
Mor-Cu-HSA-NPs	29 ± 1.5	12
Mor-Cu-PLGA-NPs	42 ± 2.0	5

less than five hydrogen donor sites and 10 acceptor sites, the molecular weight is less than 500 Da, and the log *P* value is under 5, then the compounds have drug likeliness properties. In the case of morin, the molecular weight is less than 500 Da. It has less than five hydrogen donor sites and 10 acceptor sites, and the log *P* value is under 5. This implies the existence of a drug likeliness property of morin as proposed by Lipinski's rule of five. Morin is also found to inhibit the growth of human oral squamous carcinoma cells,[36] human promyelocytic leukemia cells (HL-60),[37] etc. The chemo-preventive activity of morin against rat tongue carcinogenesis *in vitro* and *in vivo* has also been investigated.[38] Furthermore, flavonoid metal complexes like morin,[39] quercetin,[40] and chrysin[41] are found to exhibit relatively higher cytotoxic activity than the flavonoids alone. However, the therapeutic applications of flavonoids and flavonoid metal complexes are limited by their poor water solubility and low bioavailability. In the present study, we have investigated the cytotoxicity of Mor-Cu-HSA-NPs and Mor-Cu-PLGA-NPs by treating MDA-MB-468 breast cancer cells with different concentrations of NPs. Results from MTT assay showed that both the NPs (Mor-Cu-HSA-NPs and Mor-Cu-PLGA-NPs) are able to inhibit the cancer cell growth more significantly than morin and morin-Cu(II) complex. After encapsulation of the morin-Cu(II) complex into HSA-based NPs and PLGA-based NPs, the nanoparticles are able to transport and internalize higher concentrations of complex in microorganisms and cells. Thus, the NPs kill the cancer cells more effectively than morin and the morin-Cu(II) complex.

https://doi.org/10.1021/acsomega.1c06956
ACS Omega 2022, 7, 7931−7944

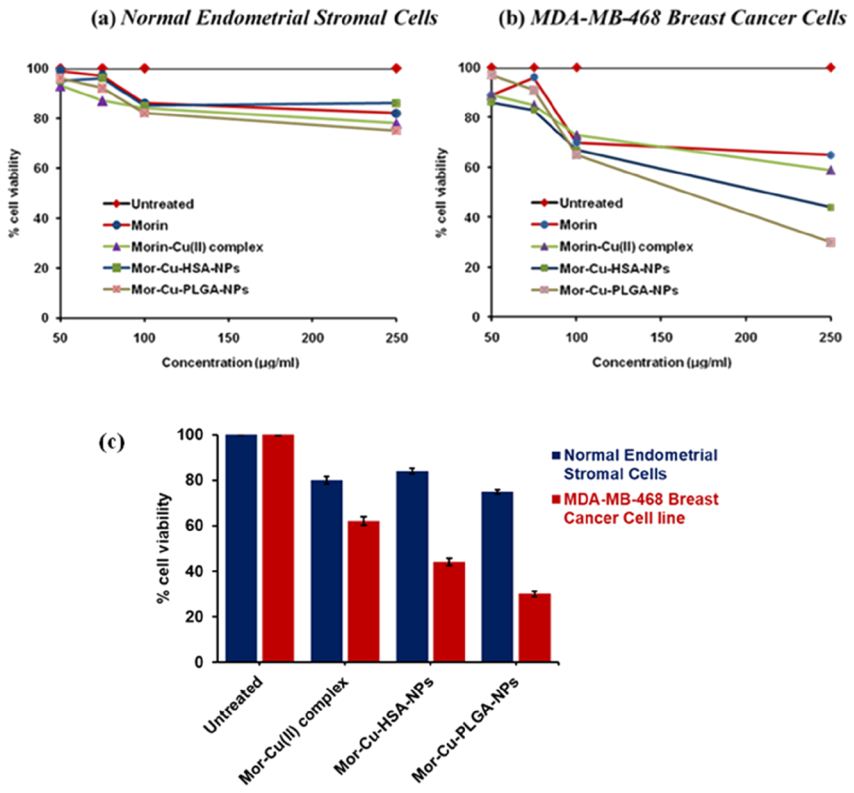

Figure 13. Cell viability plot of Mor-Cu-HSA-NPs and Mor-Cu-PLGA-NPs on (a) normal endometrial stromal cells and (b) MDA-MB-468 breast cancer cell line. (c) Histogram of cell viability of NP-treated endometrial cells and breast cancer cells at 250 μg/mL conc. of NPs.

From the results (Figure 13), it is evident that for MDA-MB-468 breast cancer cells, the cell viability was 44% for Mor-Cu-HSA-NPs and 30% for Mor-Cu-PLGA-NPs. We could not acquire normal breast cells for our study because of ethical constraints. Thus, we are not able to perform cytotoxicity tests on normal breast cells. However, we have carried out the MTT assay on normal endometrial stromal cells. Our findings suggest that treatment of normal endometrial stromal cells with both the NPs (Mor-Cu-HSA-NPs and Mor-Cu-PLGA-NPs) resulted in a cell viability of around 75%. It can be concluded that Mor-Cu-HSA-NPs and Mor-Cu-PLGA-NPs exhibit greater potency in their cytotoxic activity toward breast cancer cells with minimal or negligible effect on normal cells. From the above results, it can be further confirmed that PLGA-based NPs act as a better matrix for delivery of the morin-Cu(II) complex than HSA-based NPs.

Morphological Changes under a Microscope. To monitor the morphological changes in Mor-Cu-HSA-NP- and Mor-Cu-PLGA-NP-treated breast cancer cells, the cells were analyzed using fluorescence microscopy (Figure 14). Untreated cells retain their regular morphology when visualized under a fluorescence microscope. The green color indicates the presence of viable cells, whereas a red color is the indication of dead cells. When the treated cancer cells were taken under the fluorescence microscope, a change in the morphology of the cells occurs, which results in cellular shrinkage. We have also noted the presence of more dead cells in the case of Mor-Cu-HSA-NPs and Mor-Cu-PLGA-NPs than in the morin and the morin-Cu(II) complex alone. This observation is in agreement with the cytotoxicity results.

CONCLUSIONS

HSA-based and PLGA-based NPs have been fabricated for effective delivery of the morin-Cu(II) complex. Using a desolvation technique, Mor-Cu-HSA-NPs have been prepared and an S/O/W emulsification technique was used to obtain Mor-Cu-PLGA-NPs. Each of them possesses a spherical morphology and good encapsulation efficiency. The high negative zeta potential value of both the NPs indicates that they are sufficiently stable. The drug release profile shows a burst release in the initial period with a subsequent slow and sustained release. The non-toxic nature of both the NPs toward RBCs has also been confirmed by a hemolytic assay. An antibacterial test indicated better antibacterial activity of the Mor-Cu-PLGA-NPs in comparison with the Mor-Cu-HSA-NPs. Both the NPs showed significant cytotoxic effects on MDA-MB-468 breast cancer cell lines; only 44% cells were viable when treated with Mor-Cu-HSA-NPs, and 30% cells were viable when treated with Mor-Cu-PLGA-NPs. This implies that the PLGA-based NPs act as a better matrix than HSA-based NPs for effective delivery of the morin-Cu(II) complex. The mode of cell death was further monitored using fluorescence microscopy, and significantly more dead cells were observed in the case of NPs compared to free morin and the morin-Cu(II) complex. These results indicate that both HSA-based and PLGA-based nanoparticle systems could provide a promising therapeutic future for the morin-Cu(II) complex.

MATERIALS AND METHODS

Materials. Morin hydrate, copper acetate, PLGA (poly lactic-*co*-glycolic acid), polyvinyl alcohol (PVA), human serum albumin (HSA), and DPPH were purchased from Sigma

https://doi.org/10.1021/acsomega.1c06956
ACS Omega 2022, 7, 7931−7944

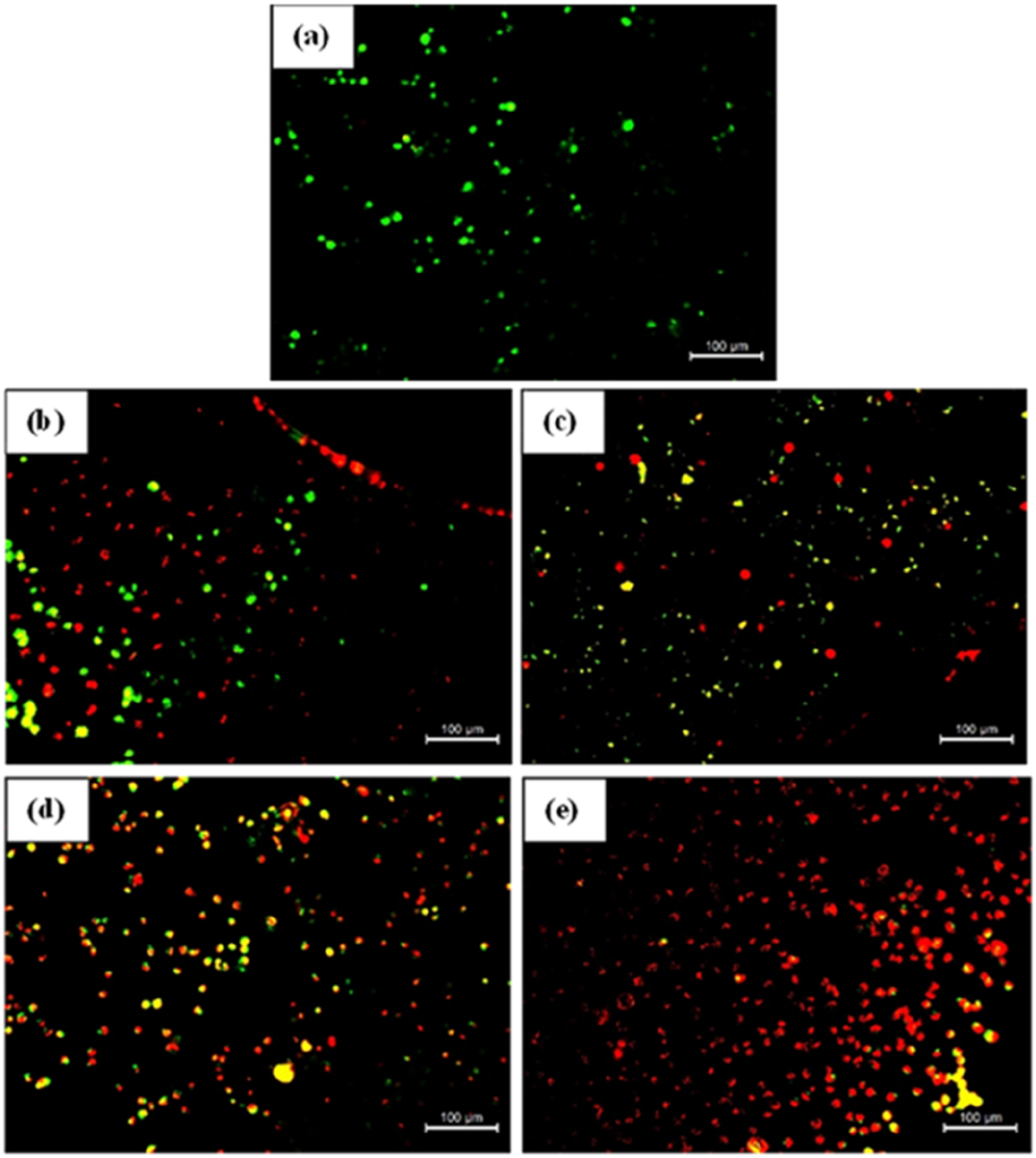

Figure 14. Fluorescence microscopy images of AO/EB dual straining of (a) untreated, (b) morin-, (c) morin-Cu(II) complex-, (d) Mor-Cu-HSA-NP-, and (e) Mor-Cu-PLGA-NP-treated MDA-MB-468 breast cancer cells after 24 h of treatment

Chemical Co. (St. Louis, USA). Dialysis bags (average flat width: 25 mm) used for *in vitro* release studies are made of cellulose membrane and were obtained from Sigma-Aldrich. The other chemicals used in these experiments were of analytical grade. The organic solvents were of HPLC grade and used as received. Milli-Q-grade water was used throughout the experiments. For cell culture studies, MDA-MB-468 breast cancer cell lines were obtained from NCCS, Pune, India. MTT (3-(4,5-dimethylthiazol-2-yl)-2,5-diphenyltetrazolium bromide) and DMSO (dimethyl sulfoxide) were purchased from Sigma Chemical Co. (St. Louis, USA). DMEM (Dulbecco's modified Eagle medium) supplemented with 10% fetal bovine serum was obtained from HIMEDIA (Mumbai, India). Cells were maintained at 37 °C in a 5% CO_2 humidified atmosphere.

Determination of Stoichiometric Ratio of the Metal and Ligand in the Complex. Job's continual variation method[42] has been applied for the determination of the stoichiometry of metal to ligand during the complexation of morin with Cu(II) in HPLC-grade ethanol. The metal-to-ligand ratio was determined by mixing both the components of equimolar concentration (1 mM) in different ratios from 1:7 to 7:1. The absorbance values were recorded at 420 nm. To determine the stoichiometric ratio between Cu(II) and morin, the absorbance at 420 nm (λ_{max}) was plotted against the mole fraction of Cu(II) ion. The breakpoint in the graph corresponds to the metal-to-morin ratio.

Synthesis of the Morin-Cu(II) Complex. The morin-Cu(II) complex was synthesized according to a previous literature report.[43] Typically, the ethanolic solution of morin

https://doi.org/10.1021/acsomega.1c06956
ACS Omega 2022, 7, 7931−7944

(0.3 g, 9.92 × 10^{-4} mol) was taken in a 50 mL round-bottomed flask and stirred at room temperature until it completely dissolved. Solid $Cu(OAc)_2 \cdot H_2O$ (0.1 g, 4.96 × 10^{-4} mol) was added to the clear brownish morin solution. The mixture was kept at room temperature, and stirring was continued for 2 h. Finally, a dark brown precipitate was formed and the reaction mixture was then filtered. The precipitate was washed with a 1:3 ethanol:H_2O mixture and kept in a vacuum desiccator to obtain the powdered form of the complex.

Characterization of the Morin-Cu(II) Complex. *Elemental Analysis.* The CHN data was obtained from a Perkin Elmer CHN Analyzer instrument.

UV−vis Spectroscopy. UV−vis spectroscopy (UV-1800, Shimadzu) was used to initially characterize the morin-Cu(II) complex. UV−vis studies were performed at 25 °C in the range 200−600 nm.

Fourier Transform Infrared Spectroscopy (FTIR) Study. FTIR spectra of the morin-Cu(II) complex were obtained on a Spectrum BX FTIR (Perkin Elmer) equipped with a lithium tantalate ($LiTaO_3$) detector and a KBr beam splitter at room temperature. The resolution used was 4 cm^{-1}, and the scanning range was from 4000 to 400 cm^{-1}.

Preparation of Morin-Cu(II) Complex-Loaded HSA NPs. The morin-Cu(II) complex-loaded HSA NPs were prepared using a desolvation technique.[17,44] Briefly, 20 mg of the morin-Cu(II) complex was incubated with 100 mg of HSA in 2.5 mL of 10 mM NaCl for 4 h at room temperature. The pH of the solution mixture was then adjusted to 8.5 by addition of NaOH. Nanoparticles were obtained by the addition of the desolvating agent ethanol drop by drop (1 mL/min) under magnetic stirring until the solution just became opaque. Then, 120 μL of 8% (v/v) glutaraldehyde was added to the mixture to stabilize the nanoparticles. The cross-linking was performed for 24 h at room temperature under constant stirring. Finally, the nanoparticles obtained were purified by centrifuging the NPs at 10,000 rpm for 15 min. The pellet was then redispersed in 10 mM NaCl in an ultrasonication bath (Oscar Ultrasonic Cleaner, Microclean-101). HSA NPs were prepared using the same approach. The NPs were then freeze-dried to obtain the powdered form. An EYELA FDU-1200 desktop-type freeze dryer equipped with a refrigerator and a vacuum pump has been used to lyophilize the NPs. The temperature and pressure were kept at −45 °C and <50 Pa, respectively.

Preparation of Morin-Cu(II) Complex-Loaded PLGA NPs. The morin-Cu(II) complex-loaded PLGA NPs were formed using a solid in oil in water (S/O/W) emulsification technique[45] with minor modifications. In this process, 50 mg of PLGA was dissolved in 1.5 mL of acetone. Ten milligrams of the morin-Cu(II) complex was then incubated with PLGA solution for 2 h at room temperature. After the incubation, the mixture was allowed to sonicate for 2 min in a bath sonicator (Oscar Ultrasonic Cleaner, Microclean-101). The morin-Cu(II) complex and PLGA in acetone were used as the organic phase, and PVA solution was used as the aqueous phase. The organic phase was then added dropwise to 3 mL of aqueous phase under magnetic stirring. The mixture was allowed to be kept under stirring conditions for 24 h. The NPs formed were then centrifuged at 6000 rpm for 15 min. The supernatant was then discarded, and the pellet was washed with Milli-Q water. The washing procedure was repeated three times. PLGA nanoparticles were also prepared using a similar technique.

Characterization of NPs. *UV−vis Spectroscopy.* Morin-Cu(II) complex-loaded HSA NPs and morin-Cu(II) complex-loaded PLGA NPs were characterized using UV−vis spectroscopy (UV-1800, Shimadzu). The measurement was done at 25 °C in a quartz cuvette of 1 cm path length. The scanning range was 200−600 nm.

Fourier Transform Infrared Spectroscopy (FTIR) Study. FTIR spectra of NPs were recorded on a Spectrum BX FTIR (Perkin Elmer) equipped with a lithium tantalate ($LiTaO_3$) detector and a KBr beam splitter at room temperature. The spectra were collected in the scanning range 4000−400 cm^{-1} with a resolution of 4 cm^{-1}.

Field Emission Scanning Electron Microscopy (FESEM). The morphological features of the nanoparticles were observed using FESEM. One droplet of the sample was applied on a cleaned glass piece and air dried. The dried samples were then coated with gold and scanned under a Carl Zeiss field emission electron microscope operating at a voltage 5 kV.

Atomic Force Microscopy (AFM). The topography of the nanoparticles was examined using AFM. The sample solutions were drop casted on a freshly cleaved mica foil and then allowed to dry in air. The images were obtained from AFM, model 5500, Agilent Technologies in tapping mode using a silicon probe cantilever of 215−235 μm length, a resonance frequency of 146−236 kHz, and a force constant of 21−98 N/m.

Determination of Particle Sizes: Dynamic Light Scattering (DLS) Study. To determine the mean particle sizes of the nanoparticles, DLS measurements were performed using a Malvern Nano ZS instrument employing a 4 mW He−Ne laser (λ = 632 nm), with a scattering angle of 173°. For the measurement, lyophilized nanoparticles were suspended in water and sonicated for 2 min to obtain a homogeneous solution, and the average particle sizes were evaluated.

Determination of Surface Charge: Zeta Potential Measurement. The surface charge of NPs was measured by means of zeta potential measurements by using a Malvern ZetaSizer Nano ZS instrument. Measurements were carried out at a scattering angle of 173° at 25 °C. The data presented here is the average of three independent readings.

Encapsulation Efficiency. The amount of the morin-Cu(II) complex entrapped in both the nanoparticles was measured using a UV−vis spectrophotometer (UV 1800, Shimadzu). Morin-Cu(II) content in both the NPs was determined by centrifuging each NP at 10,000 rpm followed by taking the absorbance of the supernatant at 420 nm (absorption maxima of the morin-Cu(II) complex). A standard calibration curve of concentration vs absorbance was plotted for each case. The encapsulation efficiency was calculated using the formula shown below:

$$\frac{W - w}{W} \times 10 \quad (1)$$

where W is the amount of the morin-Cu(II) complex initially added and w is the amount of the morin-Cu(II) complex present in the supernatant.

In Vitro Release Study. The amount of the morin-Cu(II) complex released from Mor-Cu-HSA-NPs and Mor-Cu-PLGA-NPs was quantified using a dialysis method. The experiment was performed by dispersing 6.1 mg of lyophilized NPs in 500 μL of phosphate buffer saline (PBS) (pH 7.4) and phosphate buffer (pH 6.5) and further placed in a dialysis bag (molecular weight cutoff of 12.6 kDa). The dialysis bag was then

https://doi.org/10.1021/acsomega.1c06956
ACS Omega 2022, 7, 7931−7944

immersed in 5 mL of PBS (pH 7.4) and phosphate buffer (pH 6.5) separately and stirred continuously. One milliliter of aliquots was collected at pre-fixed time intervals and replaced with the same amount of buffer. The amount of released morin-Cu(II) complex was calculated by taking the absorbance at 420 nm using UV−vis spectroscopy (UV 1800, Shimadzu).

Determination of Antioxidant Activity: DPPH Assay. To determine the antioxidant activity of the prepared NPs, 2,2-diphenyl-1-picrylhydrazyl (DPPH) assay was performed following the method described earlier.[46] For this assay, 1 mM stock DPPH solution was freshly prepared by dissolving DDPH in methanol. The Eppendorf tube was covered with aluminum foil to protect it from sunlight. Then, 100 μM DPPH solution was incubated with different concentrations of the morin, morin-Cu(II) complex, Mor-Cu-HSA-NPs, and Mor-Cu-PLGA-NPs and allowed to incubate for 30 min in the dark. The scavenging activity was estimated by recording the absorbance at 517 nm. The DPPH solution without sample was treated as the control, and ascorbic acid was taken as the standard. The percentage inhibition of DPPH was calculated according to the following equation:

$$\frac{A_{517}^{\text{control}} - A_{517}^{\text{sample}}}{A_{517}^{\text{control}}} \times 100 \quad (2)$$

where A_{517}^{control} and A_{517}^{sample} represent the absorbance of the control and sample at 517 nm, respectively.

Hemolytic Assay. A hemolytic assay was carried out to check the toxicity of the NPs.[47] In this study, fresh blood was centrifuged at 3600 rpm for 10 min. The pellet was then washed with PBS (pH 7.4), and the washing continued till the red blood cells (RBCs) were separated from the plasma and buffy coat. The NPs were then allowed to incubate with RBC suspensions (1% hematocrit) for 40 min at 37 °C. After the incubation, the sample mixtures were centrifuged at 3600 rpm for 10 min. The absorbance value of the supernatant was measured at 540 nm (the absorption maxima of hemoglobin), and the hemolytic percentage was calculated using the formula shown below:

$$\frac{A_{\text{sample}} - A_{\text{negative control}}}{A_{\text{positive control}} - A_{\text{negative control}}} \times 100 \quad (3)$$

where, A_{sample}, $A_{\text{negative control}}$, and $A_{\text{positive control}}$ represent the absorbance of the sample, negative control (PBS), and positive control (RBC in water), respectively.

Antibacterial Activity. The antibacterial activity of the prepared NPs (Mor-Cu-HSA-NPs and Mor-Cu-PLGA-NPs) was determined using a disk diffusion technique. In our present study, the activity was tested against Gram-negative bacteria *S. aureus* (MTCC96). The strain was grown overnight by inoculation in a soybean-casein digest broth at 37 °C. The culture suspensions were taken and adjusted by comparing against 0.4−0.5 McFarland turbidity standard tubes.[48] Around 20 mL of soybean-casein digest agar was poured onto sterile glass Petri dishes, and bacteria cells were inoculated homogeneously on the agar using a spreader. Paper disks (6 mm) were placed on solidified agar plates, and 10 μL of each sample was applied on the paper disk. The plates were then allowed to incubate at 37 °C for 6 h and photographed. Finally, the antibacterial potency was determined by measuring the diameter (in mm) of the inhibition zone.

Cytotoxicity Assay. The cytotoxicity of Mor-Cu-HSA-NPs and Mor-Cu-PLGA-NPs was evaluated on MDA-MB-468 breast cancer cells and primary endometrial stromal cells using the standard colorimetric MTT (3-(4,5-dimethylthiazolyl-2)-2,5-diphenyltetrazolium bromide) assay as described earlier.[49−51] Briefly, an MTT solution (10 μL) was added to the cells treated with Mor-Cu-HSA-NPs and Mor-Cu-PLGA-NPs and incubated till a purple precipitate formed. Then, DMSO (100 μL) was used to dissolve the formazan crystals and the absorbance was measured at 595 and 630 nm (reference wavelength) using a microplate absorbance reader (BIO-RAD, CA, USA). The percentage of cell viability was calculated using the following formula:

$$\frac{A_{\text{treated wells}} - A_{\text{medium control wells}}}{A_{\text{untreated wells}} - A_{\text{medium control wells}}} \times 100 \quad (4)$$

Dual Ethidium Bromide/Acridine Orange Viability Staining. Breast cancer cells were cultured on cover slips and incubated with Mor-Cu-HSA-NPs and Mor-Cu-PLGA-NPs for 24 h. A mixture of acridine orange (1 μg/mL) and ethidium bromide (1 μg/mL) solution was used to stain both the treated and untreated cells for the assessment of drug-induced apoptosis. The cells were then observed under a Leica DM 6000M microscope equipped with a fluorescence attachment, and the images were acquired with a Leica DFC 450 FX camera attached with the microscope.

Statistical Analysis. The data presented in our study have been expressed as mean ± standard deviation. All experiments have been conducted at least three times.

■ ASSOCIATED CONTENT

Supporting Information

The Supporting Information is available free of charge at https://pubs.acs.org/doi/10.1021/acsomega.1c06956.

DLS profile and zeta potential distribution of Mor-Cu-HSA-NPs and Mor-Cu-PLGA-NPs (PDF)

■ AUTHOR INFORMATION

Corresponding Author

Swagata Dasgupta − *Department of Chemistry, Indian Institute of Technology Kharagpur, Kharagpur 721302, India;* orcid.org/0000-0003-2074-1247; Phone: +91−3222-283,306; Email: swagata@chem.iitkgp.ac.in; Fax: +91−3222-282,252.

Authors

Pooja Ghosh − *Department of Chemistry, Indian Institute of Technology Kharagpur, Kharagpur 721302, India;* Present Address: Current address: Polymer Research Centre and Centre for Advanced Functional Materials, Department of Chemical Sciences, Indian Institute of Science Education and Research Kolkata, Mohanpur 741246, Nadia, West Bengal, India (P.G.)

Sudipta Bag − *Department of Chemistry, Indian Institute of Technology Kharagpur, Kharagpur 721302, India;* Present Address: Current address: Sister Nivedita University, DG Block (New Town), Action Area I, 1/2, New Town, West Bengal 700156, India (S.B.).

Sultana Parveen − *Department of Chemistry, Indian Institute of Technology Kharagpur, Kharagpur 721302, India*

Elavarasan Subramani − *School of Medical Science and Technology, Indian Institute of Technology Kharagpur,*

https://doi.org/10.1021/acsomega.1c06956
ACS Omega 2022, 7, 7931−7944

Kharagpur 721302, India; Present Address: Current address: Department of Cancer Systems Imaging, The University of Texas, MD Anderson Cancer Center, Houston, Texas, United States (E.S.)

Koel Chaudhury − *School of Medical Science and Technology, Indian Institute of Technology Kharagpur, Kharagpur 721302, India;* orcid.org/0000-0002-9390-1179

Complete contact information is available at: https://pubs.acs.org/10.1021/acsomega.1c06956

Notes

The authors declare no competing financial interest.

■ ACKNOWLEDGMENTS

S.D. is grateful to the Council of Scientific & Industrial Research (CSIR), 01(2959)/18/EMR-II. The authors would like to acknowledge the Central Research Facility, IIT Kharagpur for providing experimental facilities. The authors are also thankful to group members of Professor Koel Chaudhury (School of Medical Science and Technology, IIT Kharagpur) for providing DLS facilities and cell culture studies. P.G. and S.B. thank CSIR, New Delhi for their fellowships. S.P. thanks MHRD for her fellowship.

■ REFERENCES

(1) Kozikowski, A. P.; Tuckmantel, W.; Powis, G. Synthesis and Biological Activity of D-3-deoxy-3-fluorophosphatid-glinositol, A New Direction in the Design of non-DNA Targeted Anticancer Agent. *Angew. Chem., Int. Ed. Engl.* **1992**, *31*, 1379−1381.

(2) Tanaka, K.; Tengeiji, A.; Kato, T.; Toyama, N.; Shiro, M.; Shionoya, M. Efficient Incorporation of a Copper Hydroxylpyridine Base Pair in DNA. *J. Am. Chem. Soc.* **2002**, *124*, 12494−12498.

(3) Ming, L. J. Structure and Function of Metallo Antibiotics. *Med. Res. Rev.* **2003**, *23*, 697−762.

(4) Yaul, S. R.; Yaul, A. R.; Pethe, G. B.; Aswar, A. S. *Am-Euras. J. Sci. Res.* **2009**, *4*, 229.

(5) Panhwar, Q. K.; Memon, S. Synthesis and properties of zirconium(IV) and molybdate(II) morin complexes. *J. Coord. Chem.* **2012**, *65*, 1130−1143.

(6) Prohaska, J. R. Genetic diseases of copper metabolism. *Clin. Physiol. Biochem.* **1986**, *4*, 87−93.

(7) Shim, H.; Harris, Z. L. Genetic defects in copper metabolism. *J. Nutr.* **2003**, *133*, 1527S−1531S.

(8) Cai, L.; Li, X. K.; Song, Y.; Cherian, M. G. Essentiality, toxicology and chelation therapy of zinc and copper. *Curr. Med. Chem.* **2005**, *12*, 2753−2763.

(9) Lee, J. Y.; Moon, S. O.; Kwon, Y. J.; Rhee, S. J.; Park, H. R.; Choi, S. W. Identification and quantification of anthocyanins and flavonoids in mulberry (Morus sp.) cultivars. *Food Sci. Biotechnol.* **2004**, *13*, 176−184.

(10) Wijeratne, S. S. K.; Abou-Zaid, M. M.; Shahidi, F. Antioxidant polyphenols in almond and its coproducts. *J. Agric. Food Chem.* **2006**, *54*, 312−318.

(11) Hou, Y. C.; Chao, P. D.; Ho, H. J.; Wen, C. C.; Hsiu, S. L. Profound difference in pharmacokinetics between morin and its isomer quercetin in rats. *J. Pharm. Pharmacol.* **2003**, *55*, 199−203.

(12) Xiao, P.; Zhou, Q.; Xiao, F.; Zhao, F.; Zeng, B. Sensitive Voltammetric Determination of Morin on a Multi-Walled Carbon Nanotubes-Paraffin Oil Paste Electrode. *Int. J. Electrochem. Sci.* **2006**, *1*, 228−237.

(13) Tan, M.; Zhu, J.; Pan, Y.; Chen, Z.; Liang, H.; Liu, H.; Wang, H. Synthesis, cytotoxic activity, and DNA binding properties of copper (II) complexes with hesperetin, naringenin, and apigenin. *Bioinorg. Chem. Appl.* **2009**, *2009*, 1.

(14) Tang, H.; Wang, X.; Yang, S.; Wang, L. Synthesis, characterization, and biological activities of Pt(II) and Pd(II) complexes with 2′,3,4′,5,7-pentahydroxyflavone. *Rare Met.* **2004**, *23*, 38−42.

(15) Christie, R. J.; Grainger, D. W. Design strategies to improve soluble macromolecular delivery constructs. *Adv. Drug Delivery Rev.* **2003**, *55*, 421−437.

(16) Rajendran, L.; Knölker, H. J.; Simons, K. Subcellular targeting strategies for drug design and delivery. *Nat. Rev. Drug Discov.* **2010**, *9*, 29−42.

(17) Langer, K.; Balthasar, S.; Vogel, V.; Dinauer, N.; Von Briesen, H.; Schubert, D. Optimization of the preparation process for human serum albumin (HSA) nanoparticles. *Int. J. Pharm.* **2003**, *257*, 169−180.

(18) Singha Roy, A.; Samanta, S. K.; Ghosh, P.; Tripathy, D. R.; Ghosh, S. K.; Dasgupta, S. Cell cytotoxicity and serum albumin binding capacity of the morin−Cu(II) complex and its effect on deoxyribonucleic acid. *Mol. BioSyst.* **2016**, *12*, 2818−2833.

(19) Bukhari, S. B.; Menon, S.; Mahroof-Tahir, M.; Bhanger, M. I. Synthesis, characterization and antioxidant activity copper-quercetin complex. *Spectrochim. Acta, Part A* **2009**, *71*, 1901−1906.

(20) Rubens de Souza, F. V.; Wagner De Giovani, F. Antioxidant properties of complexes of flavonoids with metal ions. *Redox Rep.* **2004**, *9*, 97−104.

(21) Kumari, A.; Yadav, S. K.; Pakade, Y. B.; Singh, B.; Yadav, S. C. Development of biodegradable nanoparticles for delivery of quercetin. *Colloids Surf., B* **2010**, *80*, 184−192.

(22) Yadav, R.; Kumar, D.; Kumari, A.; Yadav, S. K. Encapsulation of catechin and epicatechin on BSA NPS improved their stability and antioxidant potential. *EXCLI J.* **2014**, *13*, 331−346.

(23) Ghosh, P.; Singha Roy, A.; Chaudhury, S.; Jana, S. K.; Chaudhury, K.; Dasgupta, S. Preparation of albumin based nanoparticles for delivery of fisetin and evaluation of its cytotoxic activity. *Int. J. Biol. Macromol.* **2016**, *86*, 408−417.

(24) Ghosh, P.; Bag, S.; Singha Roy, A.; Subramani, E.; Chaudhury, K.; Dasgupta, S. Solubility enhancement of morin and epicatechin through encapsulation in an albumin based nanoparticulate system and their anticancer activity against the MDA-MB-468 breast cancer cell line. *RSC Adv.* **2016**, *6*, 101415−101429.

(25) Ghosh, P.; Patwari, J.; Dasgupta, S. Complexation with Human Serum Albumin Facilitates Sustained Release of Morin From Polylactic-Co-Glycolic Acid Nanoparticles. *J. Phys. Chem. B* **2017**, *121*, 1758−1770.

(26) Schroeder, U.; Sommerfeld, P.; Ulrich, S.; Sabel, B. A. Nanoparticle technology for delivery of drugs across the blood-brain barrier. *J. Pharm. Sci.* **1998**, *87*, 1305−1307.

(27) Komatsu, H.; Kitajima, A.; Okada, S. Pharmaceutical characterization of commercially available intravenous fat emulsions: estimation of average particle size, size distribution and surface potential using photon correlation spectroscopy. *Chem. Pharm. Bull.* **1995**, *43*, 1412−1415.

(28) Jahanshahi, M.; Babaei, Z. Protein nanoparticle: A unique system as drug delivery vehicles. *Afr. J. Biotechnol.* **2008**, *7*, 4926−4934.

(29) Rother, R. P.; Bell, L.; Hillmen, P.; Gladwin, M. T. The clinical sequelae of intravascular hemolysis and extracellular plasma hemoglobin: a novel mechanism of human disease. *JAMA* **2005**, *293*, 1653−1662.

(30) Vijayababu, M. R.; Kanagaraj, P.; Arunkumar, A.; Ilangovan, R.; Dharmarajan, A.; Arunakaran, J. Quercetin induces p53-independent apoptosis in human prostate cancer cells by modulating Bcl-2-related proteins: a possible mediation by IGFBP-3. *Oncol. Res.* **2006**, *16*, 67−74.

(31) Yang, P. M.; Tseng, H. H.; Peng, C. W.; Chen, W. S.; Chiu, S. J. Dietary flavonoid fisetin targets caspase-3-deficient human breast cancer MCF-7 cells by induction of caspase-7-associated apoptosis and inhibition of autophagy. *Int. J. Oncol.* **2012**, *40*, 469−478.

(32) Choi, S. I.; Jeong, C. S.; Cho, S. Y.; Lee, Y. S. Mechanism of Apoptosis Induced by Apigenin in HepG2 Human Hepatoma Cells:

Involvement of Reactive Oxygen Species Generated by NADPH Oxidase. *Arch. Pharmacal Res.* **2007**, *30*, 1328−1335.
(33) Louis Jeune, M. A.; Kumi-Diaka, J.; Brown, J. Anticancer activities of pomegranate extracts and genistein in human breast cancer cells. *J. Med. Food* **2005**, *8*, 469−475.
(34) Lin, Y.; Shi, R.; Wang, X.; Shen, H. M. Luteolin, a flavonoid with potential for cancer prevention and therapy. *Curr. Cancer Drug Targets* **2008**, *8*, 634−646.
(35) Lipinski, C. A. Lead and drug-like compounds: the rule-of-five revolution. *Drug Discov. Today: Technol.* **2004**, *1*, 337−341.
(36) Brown, J.; O'Prey, J.; Harrison, P. R. Enhanced sensitivity of human oral tumors to the flavonol, morin, during cancer progression: involvement of the Akt and stress kinase pathways. *Carcinogenesis* **2003**, *24*, 171−177.
(37) Kuo, H. M.; Chang, L. S.; Lin, Y. L.; Lu, H. F.; Yang, J. S.; Lee, J. H.; Chung, J. G. Morin inhibits the growth of human leukemia HL-60 cells via cell cycle arrest and induction of apoptosis through mitochondria dependent pathway. *Anticancer Res.* **2007**, *27*, 395−405.
(38) Kawabata, K.; Tanaka, T.; Honjo, S.; Kakumoto, M.; Hara, A.; Makita, H.; Tatematsu, N.; Ushida, J.; Tsuda, H.; Mori, H. Chemopreventive effect of dietary flavonoid morin on chemically induced rat tongue carcinogenesis. *Int. J. Cancer* **1999**, *83*, 381−386.
(39) Song, Y. M.; Kang, J. W.; Wang, Z. H.; Lua, X. Q.; Gao, J. Z.; Wang, L. F. Study on the interactions between CuL and Morin with DNA. *J. Inorg. Biochem.* **2002**, *91*, 470−474.
(40) Zhou, J.; Wang, L.-F.; Wang, J.-Y.; Tang, N. Synthesis, characterization, antioxidative and antitumor activities of solid quercetin rare earth(III) complexes. *J. Inorg. Biochem.* **2001**, *83*, 41−48.
(41) Zeng, Y.-B.; Yang, N.; Liu, W.-S.; Tang, N. Synthesis, characterization and DNA-binding properties of La(III) complex of chrysin. *J. Inorg. Biochem.* **2003**, *97*, 258−264.
(42) Harris, D. C. *Quantitative Chemical Analysis*; Freeman W.H. and Company Publisher: New York, USA, Seventh Edition., 1995.
(43) Zhang, Q.; Wang, L.; Liu, X. Synthesis, characterization and antitumour properties of metal(II) solid complexes with morin. *Transition Met. Chem.* **1996**, *21*, 23−27.
(44) Weber, C.; Kreuter, J.; Langer, K. Desolvation process and surface characteristics of HSA-nanoparticles. *Int. J. Pharm.* **2000**, *196*, 197−200.
(45) Xie, X.; Tao, Q.; Zou, Y.; Zhang, F.; Guo, M.; Wang, Y.; Wang, H.; Zhou, Q.; Yu, S. PLGA nanoparticles improve the oral bioavailability of curcumin in rats: characterizations and mechanisms. *J. Agric. Food Chem.* **2011**, *59*, 9280−9289.
(46) Zhang, Y.; Yang, Y.; Tang, K.; Hu, X.; Zou, G. Physicochemical characterization and antioxidant activity of quercetin-loaded chitosan nanoparticles. *J. Appl. Polym. Sci.* **2008**, *107*, 891−897.
(47) Vedakumari, W. S.; Priya, V. M.; Sastry, T. P. Deposition of superparamagnetic nanohydroxyapatite on iron-fibrin substrates: preparation, characterization, cytocompatibility and bioactivity studies. *Colloids Surf., B* **2014**, *120*, 208−214.
(48) McFarland, J. Nephelometer: An Instrument for Estimating the Number of Bacteria in Suspensions Used for Calculating the Opsonic Index and for Vaccines. *JAMA* **1907**, *XLIX*, 1176−1178.
(49) Uboldi, C.; Bonacchi, D.; Lorenzi, G.; Hermanns, M. I.; Pohl, C.; Baldi, G.; Unger, R. E.; Kirkpatrick, C. J. Gold nanoparticles induce cytotoxicity in the alveolar type-II cell lines A549 and NCIH441. *Part Fibre Toxicol.* **2009**, *6*, 18.
(50) Satyavani, K.; Gurudeeban, S.; Ramanathan, T.; Balasubramanian, T. Toxicity study of silver nanoparticles synthesized from Suaeda monoica on Hep-2 cell line. *Avicenna J. Med. Biotechnol.* **2012**, *4*, 35−39.
(51) Chen, H.; Zhang, X.; Dai, S.; Ma, Y.; Cui, S.; Achilefu, S.; Gu, Y. Multifunctional gold nanostar conjugates for tumor imaging and combined photothermal and chemo-therapy. *Theranostics* **2013**, *3*, 633−649.

https://doi.org/10.1021/acsomega.1c06956
ACS Omega 2022, 7, 7931−7944